cancers

MDPI

Article

Tumor-Infiltrating and Circulating CD103-Expressing T Cells Show Distinct Lineage-Specific Clinical Associations in Head and Neck Squamous Cell Carcinoma

Hideyuki Takahashi *, Miho Uchida, Hiroe Tada, Hiroyuki Hagiwara and Kazuaki Chikamatsu

Department of Otolaryngology-Head and Neck Surgery, Gunma University Graduate School of Medicine, 3-39-22 Showa-machi, Maebashi 371-8511, Gunma, Japan

* Correspondence: htakahas@gunma-u.ac.jp; Tel.: +81-27-220-8350

Simple Summary

Tissue-resident memory T cells are immune cells that remain in tissues and can contribute to antitumor immune responses. CD103 is commonly used to identify these cells, but CD103-expressing T cells may have different roles depending on the type of T cell and whether they are found in the tumor or blood. We investigated CD103-expressing T cells in head and neck squamous cell carcinoma using tumor gene-expression data and direct analysis of T cells from tumors and peripheral blood. Higher levels of CD103-expressing $CD8^+$ T cells in tumors showed a possible association with better clinical outcomes, whereas CD103-expressing T cells in blood showed different clinical associations. In patients with paired blood and tumor samples, it remained unclear how closely the proportion of CD103-expressing T cells in blood tracked the proportion in the tumor. These findings highlight the importance of considering both T-cell type and anatomical location when evaluating CD103-expressing T cells as potential biomarkers of antitumor immunity.

Abstract

Background/Objectives: CD103 is associated with tissue-resident memory T (T_{RM}) cells and antitumor immunity, but its clinical significance may differ by T-cell lineage and anatomical compartment. We investigated the clinical and immunological significance of CD103-expressing T cells in head and neck squamous cell carcinoma (HNSCC) across tumor and peripheral blood compartments. **Methods:** Transcriptomic data from 520 HNSCC cases in The Cancer Genome Atlas (TCGA) were analyzed using *CD4* or *CD8A* expression combined with *ITGAE* expression, followed by survival and immune analyses. $CD4^+CD103^+$ and $CD8^+CD103^+$ T cells were evaluated by flow cytometry in tumor-infiltrating lymphocytes (TILs; n = 39) and peripheral blood mononuclear cells (PBMCs; n = 89), including paired samples from 18 patients. **Results:** In the TCGA cohort, *ITGAE*-high tumors exhibited immunologically active but heterogeneous microenvironments, characterized by concurrent enrichment of effector-associated and immunoregulatory features. In TILs, a higher proportion of $CD8^+CD103^+$ T cells showed a nominal association with a lower hazard of progression or death after adjustment for TNM stage and showed distinct immunophenotypic associations. In contrast, a higher proportion of circulating $CD4^+CD103^+$ T cells showed a nominal association with a higher hazard. In paired samples, both $CD4^+CD103^+$ and $CD8^+CD103^+$ T-cell frequencies were higher in TILs than in PBMCs, with no significant correlation between peripheral and intratumoral frequencies. **Conclusions:** Our findings suggest a possible prognostic role for selected CD103-

Academic Editor: Orlando Guntinas-Lichius

Received: 9 October 2026
Revised: 25 November 2026
Accepted: 26 November 2026
Published: 28 November 2026

Copyright: © 2026 by the authors. Licensee MDPI, Basel, Switzerland. This article is an open access article distributed under the terms and conditions of the Creative Commons Attribution (CC BY) license.

expressing T-cell populations in HNSCC. Larger studies with paired tumor and blood samples are needed to assess whether their associations with progression-free survival differ by T-cell lineage or sampling compartment.

Keywords: head and neck squamous cell carcinoma; CD103; tissue-resident memory T cells; tumor-infiltrating lymphocytes; peripheral blood; $CD8^+$ T cells; $CD4^+$ T cells; tumor immune microenvironment

1. Introduction

Head and neck squamous cell carcinoma (HNSCC) is a heterogeneous malignancy arising from the mucosal epithelium of the upper aerodigestive tract [1–3]. Despite advances in multimodal treatment and the introduction of immune checkpoint inhibitors, clinical outcomes remain variable, reflecting substantial heterogeneity in both tumor biology and host antitumor immunity [3,4]. The immune microenvironment is increasingly recognized as an important determinant of disease progression and therapeutic response in HNSCC, with tumor-infiltrating T cells playing a central role in antitumor immune responses [5,6]. However, the clinical significance of T-cell infiltration depends not only on the abundance of T cells but also on their differentiation state, functional properties, and localization within the tumor microenvironment [7–9]. Defining T-cell populations that reflect effective local antitumor immunity may therefore provide important insights into the immunobiology and clinical behavior of HNSCC.

Tissue-resident memory T (T_{RM}) cells are a distinct population of memory T cells that persist within peripheral tissues and contribute to local immune surveillance without continuous recirculation through the bloodstream [10,11]. Among the molecules associated with tissue residency, CD103, encoded by *ITGAE*, is widely used as a marker of T_{RM} cells, particularly in epithelial tissues [12]. CD103 forms the $\alpha E\beta 7$ integrin and interacts with E-cadherin expressed by epithelial cells, thereby contributing to the retention and positioning of T cells within tissues [12,13]. In solid tumors, CD103-expressing $CD8^+$ T cells have been associated with enhanced local antitumor immunity and favorable clinical outcomes in multiple cancer types, including HNSCC [14–17]. However, tumor-infiltrating T_{RM}-like cells can also express inhibitory receptors and exhibit features of dysfunction, suggesting that CD103 expression does not necessarily define a functionally uniform T-cell population [17].

Despite growing evidence supporting the clinical relevance of $CD103^+$ T cells in solid tumors, important questions remain regarding the influence of T-cell lineage and anatomical compartment. Most studies have focused on $CD8^+CD103^+$ T cells, whereas CD103 is also expressed by subsets of $CD4^+$ T cells, including regulatory T cells [18,19]. The clinical and immunological significance of CD103 expression may therefore differ between $CD4^+$ and $CD8^+$ T cells. Moreover, whether circulating $CD103^+$ T cells reflect their intratumoral counterparts remains unclear. Because tissue residency is shaped by local microenvironmental signals and retention mechanisms, circulating $CD103^+$ T cells cannot necessarily be considered equivalent to intratumoral $CD103^+$ T cells [20,21]. Nevertheless, peripheral blood provides an accessible source for immune monitoring, underscoring the importance of defining the relationship between circulating and intratumoral $CD103^+$ T-cell populations. Systematic evaluation across T-cell lineages and anatomical compartments may therefore provide a more comprehensive understanding of the clinical and immunological significance of CD103 in HNSCC.

In this study, we investigated the clinical and immunological significance of CD103-expressing T cells in HNSCC using complementary transcriptomic and cellular

approaches. We first analyzed The Cancer Genome Atlas (TCGA) transcriptomic data to characterize the prognostic and immune features associated with *ITGAE* expression in the context of *CD4* and *CD8A* expression. We then directly evaluated $CD4^+CD103^+$ and $CD8^+CD103^+$ T cells among tumor-infiltrating lymphocytes (TILs) and peripheral blood mononuclear cells (PBMCs) using flow cytometry and examined their associations with clinical outcomes and immunophenotypic characteristics. Finally, paired peripheral blood and tumor samples were analyzed to determine the relationship between circulating and intratumoral $CD103^+$ T-cell frequencies. Through this integrated approach, we aimed to clarify how the clinical and immunological significance of CD103 expression differs according to T-cell lineage and anatomical compartment.

2. Materials and Methods

2.1. Acquisition of TCGA Dataset

Gene expression data (Illumina HiSeq RNA-seq V2 normalized counts) and corresponding clinical information for 520 patients with HNSCC were retrieved from TCGA via the FireBrowse portal (http://firebrowse.org/). The dataset included 97 human papillomavirus (HPV)-positive and 423 HPV-negative tumors.

2.2. Patient Stratification Based on CD4/CD8A and ITGAE Expression

Tumor samples were stratified based on the expression levels of T cell–related markers. For each gene, expression values were standardized across the 520 tumors using z-score normalization. Patients were classified separately according to *CD4*/*ITGAE* or *CD8A*/*ITGAE* expression using a fixed z-score threshold of 0. Tumors with *CD4* or *CD8A* z-scores below 0 were classified as CD4lo or CD8lo, respectively, regardless of *ITGAE* expression. Tumors with *CD4* or *CD8A* z-scores of 0 or higher were further classified according to *ITGAE* expression, yielding CD4hiITGAElo and CD4hiITGAEhi groups or CD8hiITGAElo and CD8hiITGAEhi groups. *ITGAE*-low and *ITGAE*-high status were defined using the same z-score threshold of 0. The z-score threshold of 0 was used as an outcome-independent operational cutoff for exploratory stratification rather than as a biologically validated boundary between distinct expression populations. We used these groups to display Kaplan–Meier curves and to compare pathway enrichment, immune-cell composition, and T-cell-related transcriptional signatures. The distributions of *CD4*, *CD8A*, and *ITGAE* expression across the TCGA cohort were visualized using kernel density plots (Figure S1E). Kaplan–Meier survival curves were generated to compare progression-free survival (PFS) and overall survival (OS) among the three groups, and differences were assessed using the log-rank test.

Survival associations were assessed using Cox proportional hazards regression models, with PFS as the primary endpoint and OS as the secondary endpoint. The overarching hypothesis that CD103-associated T-cell populations are associated with survival outcomes was established a priori. Each gene and clinical covariate was first analyzed separately in a univariable model. Continuous expression of *ITGAE* was then analyzed jointly with either *CD4* or *CD8A* expression in separate multivariable models adjusted for TNM stage, HPV status, and primary tumor site. Hazard ratios (HRs) and 95% confidence intervals (CIs) were calculated. For gene expression, HRs were reported per one standard deviation increase. To account for multiple testing, the Benjamini–Hochberg false discovery rate (FDR) procedure was applied to the four *p*-values for the gene-expression coefficients in the two multivariable models (*CD4* and *ITGAE* in one model and *CD8A* and *ITGAE* in the other). Both nominal and FDR-adjusted *p*-values were reported.

2.3. Gene Set Enrichment Analysis (GSEA)

Differential expression was analyzed using limma (version 3.60.6) with log10-transformed RSEM-normalized expression values [log10(x + 1)]. CD4hiITGAEhi and CD8hiITGAEhi tumors were each compared with their respective remaining groups, adjusting for HPV status, primary tumor site, and TNM stage. Each of the 20,531 rows in the original expression matrix had a unique Entrez Gene ID. These IDs were used for gene ranking and matching to Hallmark gene sets, preserving distinct genes that shared a gene symbol. After excluding the 269 genes with constant expression across all 520 tumors, the remaining 20,262 genes were ranked by limma moderated t-statistics obtained with empirical Bayes mean–variance trend adjustment. Pre-ranked GSEA was performed using fgseaMultilevel (fgsea version 1.30.0) with human Hallmark gene sets obtained through msigdbr (version 26.1.0). Gene set sizes were restricted to 15–500 genes, with eps = 0 and a random seed of 20261030. Benjamini–Hochberg correction was applied within the Hallmark collection separately for each comparison, with adjusted $p < 0.05$ considered significant.

2.4. Immune Cell Composition Analysis Using CIBERSORTx

The immune composition of the tumor microenvironment was estimated from bulk RNA-sequencing data using CIBERSORTx [22]. The LM22 signature matrix was used to estimate the relative abundance of 22 immune cell populations. RSEM-normalized expression values were supplied on the linear scale without log transformation. CIBERSORTx was run in both relative and absolute modes with 100 permutations, with quantile normalization disabled and no batch correction. All 520 tumors were included regardless of the deconvolution *p* value.

In relative mode, the estimated fractions of the 22 LM22 cell types summed to one within each tumor. For each classification (*CD4*/*ITGAE* and *CD8A*/*ITGAE*), we compared the overall 22-cell-type composition across the three groups using permutational multivariate analysis of variance (PERMANOVA) based on Hellinger distances. We also assessed differences in multivariate dispersion using distances to group spatial medians. Both tests used 9999 permutations. PERMANOVA *p* values were adjusted across the two classifications using the Benjamini–Hochberg method. In absolute mode, we compared cell type–specific CIBERSORTx scores, expressed in arbitrary units, using two-sided pairwise Welch's *t*-tests. For each cell type, we estimated mean score differences and 95% confidence intervals for all three pairwise comparisons within each classification. We applied the Benjamini–Hochberg method across all 132 comparisons (22 cell types × 3 pairwise comparisons × 2 classifications).

2.5. T-Cell Functional Signature Analysis

Gene expression-based scores were calculated to characterize T-cell functional states within the TCGA tumors. Four non-overlapping signatures—exhaustion, cytotoxicity, proliferation, and a tissue-resident memory (T_{RM}) core signature excluding *ITGAE*—were evaluated. For each gene, log10-transformed RSEM-normalized expression values were standardized across all 520 samples using z-score normalization, and each signature score was calculated as the mean of the corresponding gene-wise z-scores. The genes and references used for each signature are provided in Supplementary Table S1.

Differences among the three *CD4*/*ITGAE*- or *CD8A*/*ITGAE*-based groups were assessed using one-way ANOVA followed by Tukey's HSD test. Benjamini–Hochberg FDR correction was applied to the four ANOVA tests within each classification and, separately, across all 24 Tukey-adjusted pairwise comparisons. Correlations among signature scores were assessed using Spearman's rank correlation coefficient.

2.6. Patient Cohorts and Sample Collection

Patients with HNSCC who were newly diagnosed and treated at Gunma University Hospital (Maebashi, Japan) were enrolled for flow cytometric analyses. Patients with a history of other malignancies, autoimmune disorders, chronic infectious diseases, or hematological conditions, as well as those receiving immunomodulatory therapies, were excluded. HPV status was assessed using p16 immunohistochemistry as a surrogate marker. Of the 89 patients included in the PBMC cohort, 60 had been included in our previous study focusing on CD69-expressing T cells [15]. The remaining 29 patients were newly included in the present cohort. Unlike the previous study, the present investigation evaluated CD103 expression and its associations with multiple T-cell phenotypic markers. Clinical information was obtained from electronic medical records, and tumor staging was determined according to the eighth edition of the TNM classification system. For the TIL cohort, follow-up for PFS and OS began on the date of surgery, when the tumor specimen was collected. For the PBMC cohort, follow-up began on the date of diagnosis, and all blood samples were collected before treatment initiation. PFS was measured from the cohort-specific time origin to the first occurrence of disease recurrence, disease progression, or death from any cause. Patients without a PFS event were censored at the date of their last disease assessment.

PBMCs were isolated from whole blood by density gradient centrifugation using Ficoll-Paque PLUS (GE Healthcare, Pittsburgh, PA, USA). Fresh tumor specimens were obtained from surgically resected HNSCC tissues and processed for isolation of TILs. Tumor tissues were mechanically and enzymatically dissociated using the Tumor Dissociation Kit, human (Miltenyi Biotec, Bergisch Gladbach, Germany) in combination with the gentleMACS Dissociator (Miltenyi Biotec), according to the manufacturer's protocol. Briefly, fat, fibrous tissue, and necrotic areas were removed, and tumor specimens were minced into 2–4-mm pieces before enzymatic digestion and mechanical dissociation. The resulting cell suspension was passed through a 70-μm MACS SmartStrainer (Miltenyi Biotec) and washed with RPMI 1640. Erythrocytes were removed using RBC Lysis Buffer (Roche, Basel, Switzerland). Among these patients, paired PBMC and TIL samples obtained from the same individuals were available in 18 cases and were used for paired analyses.

This study was approved by the Institutional Review Board of Gunma University (HS2017-152), and written informed consent was obtained from all participants prior to sample collection.

2.7. Flow Cytometry

TILs and PBMCs were subjected to flow cytometric analysis. Prior to staining, Fc receptors were blocked with BD Fc Block™ (BD Biosciences, San Jose, CA, USA) to minimize nonspecific antibody binding. Cells were subsequently incubated with fluorochrome-conjugated monoclonal antibodies against human surface markers (listed in Supplementary Table S2). Staining was carried out at 4 °C for 45 min in the dark using phosphate-buffered saline supplemented with 1% heat-inactivated fetal calf serum (Thermo Fisher Scientific, Waltham, MA, USA) and 0.1% sodium azide (Sigma-Aldrich, St. Louis, MO, USA). For intracellular staining, cells were fixed and permeabilized using the Foxp3/Transcription Factor Staining Buffer Set (Thermo Fisher Scientific) according to the manufacturer's instructions. TIL samples were acquired using an Attune NxT Flow Cytometer (Thermo Fisher Scientific), whereas PBMC samples were acquired using a BD FACSVerse flow cytometer (BD Biosciences). Subsequent analyses were conducted using FlowJo software (Tree Star, Ashland, OR, USA). Fluorescence compensation matrices were generated using UltraComp eBeads Compensation Beads (Thermo Fisher Scientific). For PBMC analyses, debris and events with abnormal forward- and side-scatter characteristics were excluded based on FSC-A and SSC-A. The PBMC panel did not include a viability dye. For TIL analyses, dead cells were excluded using LIVE/DEAD Fixable Aqua viability staining.

Doublets were excluded using the gating strategies illustrated in Supplementary Figures S2 and S3. Only samples containing more than 10,000 cells after the exclusion gates were included in the analyses. Representative gating strategies and definitions of T-cell subsets are provided in Supplementary Figures S2 and S3.

2.8. Survival Analysis in the TIL and PBMC Cohorts

The prognostic significance of $CD4^+CD103^+$ and $CD8^+CD103^+$ T-cell populations was evaluated separately in the TIL and PBMC cohorts. The proportions of $CD103^+$ cells among $CD4^+$ and $CD8^+$ T cells were analyzed as continuous variables in Cox proportional hazards regression models, without dichotomization or outcome-derived cutoff optimization. Hazard ratios (HRs) were expressed per 10-percentage-point increase in $CD103^+$ T-cell proportions for the TIL cohort and per 1-percentage-point increase for the PBMC cohort. PFS and OS were analyzed separately.

$CD4^+CD103^+$ and $CD8^+CD103^+$ T-cell proportions were evaluated in separate Cox models. Multivariable analyses were adjusted for overall TNM stage, which was selected as a clinically relevant prognostic factor rather than on the basis of univariate statistical significance. Stage was categorized as II–III versus IV in the TIL cohort and I–II versus III–IV in the PBMC cohort. The adjusted models were deliberately kept parsimonious because of the limited number of survival events, particularly in the TIL cohort. In addition, the distributions of clinicopathological characteristics were imbalanced, particularly in the TIL cohort, in which all patients were HPV-negative and 35 of 39 patients had hypopharyngeal cancer. Therefore, additional clinicopathological variables were not included in the multivariable models. To account for multiple testing, *p*-values for the $CD4^+CD103^+$ and $CD8^+CD103^+$ T-cell proportions in the TNM stage-adjusted Cox models were corrected using the Benjamini–Hochberg FDR procedure separately for PFS and OS within each cohort.

The proportional hazards assumption was assessed using Schoenfeld residuals. Given the limited number of events, particularly for OS, the stability and interpretability of the adjusted Cox estimates were carefully considered, and the survival analyses were regarded as exploratory.

2.9. Association Between CD103-Related Variables and Clinicopathological Characteristics

Associations between *CD4*/*ITGAE*- and *CD8A*/*ITGAE*-based classifications and clinicopathological characteristics were examined separately in the TCGA cohorts using Pearson's chi-squared test or Fisher's exact test, as appropriate. In the TIL and PBMC cohorts, the proportions of $CD103^+$ cells among $CD4^+$ and $CD8^+$ T cells were analyzed as continuous variables. Differences in these proportions according to clinicopathological characteristics were assessed using the Wilcoxon rank-sum test for comparisons between two groups and the Kruskal–Wallis test for comparisons among three or more groups. To account for multiple testing, *p*-values were adjusted using the Benjamini–Hochberg procedure, and FDR-adjusted *p*-values were reported for all three cohorts.

2.10. Correlation Analysis of $CD103^+$ T Cells and T-Cell Phenotypes

Associations between the proportions of $CD103^+$ cells and other T-cell phenotypes were evaluated separately for the $CD4^+$ and $CD8^+$ compartments. Parameters included expression of immune checkpoint molecules (PD-1, TIM-3, CTLA-4, TIGIT, and LAG-3), CD38, Ki-67, and naïve and memory T-cell subsets. Spearman's rank correlation coefficient was used as the primary measure of correlation. To account for multiple testing, *p*-values were adjusted using the Benjamini–Hochberg procedure, and the resulting adjusted *p*-values were interpreted as FDR-adjusted *p*-values.

2.11. Paired Comparison of Peripheral Blood and Tumor-Infiltrating T Cells

For patients with paired PBMC and TIL samples, the proportions of $CD4^+CD103^+$ and $CD8^+CD103^+$ T cells were compared between the peripheral blood and tumor compartments. Paired comparisons of T-cell parameters between PBMCs and TILs were performed using the Wilcoxon signed-rank test. *p*-values were adjusted using the Benjamini–Hochberg method, and FDR-adjusted *p*-values < 0.05 were considered statistically significant. The relationships between peripheral and intratumoral $CD103^+$ T-cell frequencies were additionally assessed using Spearman's rank correlation analysis. For the $CD4^+$ and $CD8^+$ T-cell subsets, we estimated 95% confidence intervals for Spearman's ϱ using the percentile bootstrap method with 10,000 patient-level resamples, keeping each patient's blood and tumor measurements paired. *p*-values from the correlation analyses were adjusted for multiple testing using the Benjamini–Hochberg method.

2.12. Statistical Analysis

All statistical analyses were performed using R software (version 4.3.1; R Foundation for Statistical Computing, Vienna, Austria). Unless otherwise specified, all statistical tests were two-sided, and $p < 0.05$ was considered statistically significant.

3. Results

3.1. Survival Associations and Immune Characteristics of CD4, CD8A, and ITGAE Expression in TCGA-HNSCC

To investigate the clinical and immunological significance of *CD4*/*CD8A*- and *ITGAE*-associated T-cell states in HNSCC, we first analyzed RNA-sequencing data from 520 patients in the TCGA cohort. Tumors were stratified into three groups according to *CD4* and *ITGAE* expression (CD4lo, $n = 248$; CD4hiITGAElo, $n = 111$; and CD4hiITGAEhi, $n = 161$) or *CD8A* and *ITGAE* expression (CD8lo, $n = 248$; CD8hiITGAElo, $n = 94$; and CD8hiITGAEhi, $n = 178$) using fixed z-score thresholds (Figure 1A,B). The expression distributions of *CD4*, *CD8A*, and *ITGAE* were predominantly unimodal, with no clearly separated expression populations (Figure S1E). The mean and median expression values were similar for each gene (*CD4*: 2.848 and 2.869; *CD8A*: 2.168 and 2.194; *ITGAE*: 2.504 and 2.498, respectively), indicating that the z-score threshold of 0 was located near the center of each distribution. Of the 520 patients, 429 had evaluable PFS data (126 events) and 495 had evaluable OS data (190 deaths). Follow-up time and event status were both missing for 91 patients for PFS and 25 for OS. Fisher's exact tests showed no statistically significant association between endpoint availability and the three-group expression classifications for either PFS (*CD4*-based, $p = 0.888$; *CD8A*-based, $p = 0.229$) or OS (*CD4*-based, $p = 0.061$; *CD8A*-based, $p = 0.256$). Kaplan–Meier analyses showed no statistically significant differences in PFS or OS among the *CD4*-based groups (Figure 1C). Similarly, neither PFS nor OS differed significantly among the *CD8A*-based groups (Figure 1D).

In univariable analysis, the HR for progression or death per SD increase in *ITGAE* expression was 1.139 (95% CI, 0.965–1.345; $p = 0.123$). After adjustment for *CD4* expression, HPV status, primary tumor site, and TNM stage, higher *ITGAE* expression was associated with a higher hazard of progression or death (HR, 1.292; 95% CI, 1.087–1.536; nominal $p = 0.004$; FDR-adjusted $p = 0.007$). The estimate was similar when *CD8A* replaced *CD4* in the model (HR, 1.318; 95% CI, 1.099–1.582; nominal $p = 0.003$; FDR-adjusted $p = 0.007$). Higher *CD4* expression was associated with a lower hazard in the *CD4* model (HR, 0.819; 95% CI, 0.689–0.972; FDR-adjusted $p = 0.030$). The corresponding estimate for *CD8A* was 0.842 (95% CI, 0.697–1.018; FDR-adjusted $p = 0.076$). HPV-positive status was associated with a lower hazard of progression or death and advanced TNM stage with a higher hazard in both models (Table 1). For OS, none of the four gene-expression coefficients was

statistically significant after FDR correction. Advanced TNM stage was associated with a higher hazard of death in both models (Table S3).

We next examined the biological characteristics associated with *ITGAE* expression. GSEA demonstrated enrichment of multiple immune-related Hallmark pathways in both CD4hiITGAEhi and CD8hiITGAEhi tumors compared with their respective remaining groups, including interferon responses, inflammatory response, IL2–STAT5 signaling, and allograft rejection (Figure 1E,F). Across all 520 tumors, the relative profiles of the 22 LM22 immune cell types were associated with both the *CD8A*/*ITGAE* classification (PERMANOVA $R^2 = 0.114$) and the *CD4*/*ITGAE* classification ($R^2 = 0.072$), with a Benjamini–Hochberg-adjusted p value of 0.0001 for each. Group mean relative fractions are shown in Figure 1G and Figure S1A, respectively. Within-group dispersion also differed across groups for both classifications ($p = 0.0001$ for each). In absolute mode, CD8hiITGAEhi tumors had higher mean scores for $CD8^+$ T cells, activated $CD4^+$ memory T cells, follicular helper T cells, regulatory T cells, and M1 and M2 macrophages than CD8lo tumors. Mean scores for M0 macrophages and activated mast cells were lower in CD8hiITGAEhi tumors (Figure 1H). The corresponding comparison of CD4hiITGAEhi and CD4lo tumors showed the same pattern for seven of the eight cell types, with no significant difference in M0 macrophage scores between the two groups (Figure S1B). These findings suggest that CD8hiITGAEhi and CD4hiITGAEhi tumors are characterized by a heterogeneous immune microenvironment containing both effector-associated and immunoregulatory cell populations. Consistent with these differences in immune-cell composition, T-cell-related transcriptional signature analysis revealed significant differences in exhaustion, cytotoxicity, proliferation, and T_{RM} core scores among both the *CD4*/*ITGAE*- and *CD8A*/*ITGAE*-based groups (Figure 1I,J and Figure S1C,D). The *ITGAE*-high groups generally exhibited higher signature scores. Although the four signatures contained no overlapping genes, exhaustion, cytotoxicity, and T_{RM} core scores were strongly correlated (Spearman's ρ = 0.881–0.920), whereas proliferation showed weaker correlations with the other signatures (ρ = 0.098–0.122). These findings suggest that the correlated signatures may reflect shared immune-related transcriptional programs rather than independent evidence of distinct T-cell functional states.

Finally, the relationships between the *CD4*/*CD8A*- and *ITGAE*-based classifications and clinicopathological characteristics were examined (Table S4). Both *CD4*- and *CD8A*-based classifications were significantly associated with HPV status and primary tumor site. In addition, the *CD8A*-based classification was significantly associated with T factor and TNM stage, whereas the *CD4*-based classification was not. These findings indicate that the *CD4*/*ITGAE*- and *CD8A*/*ITGAE*-based classifications are associated with distinct clinicopathological features of HNSCC. Collectively, the TCGA analyses suggest that *ITGAE*-high tumors exhibit immunologically active but heterogeneous microenvironments, characterized by concurrent enrichment of effector-associated and immunoregulatory features.

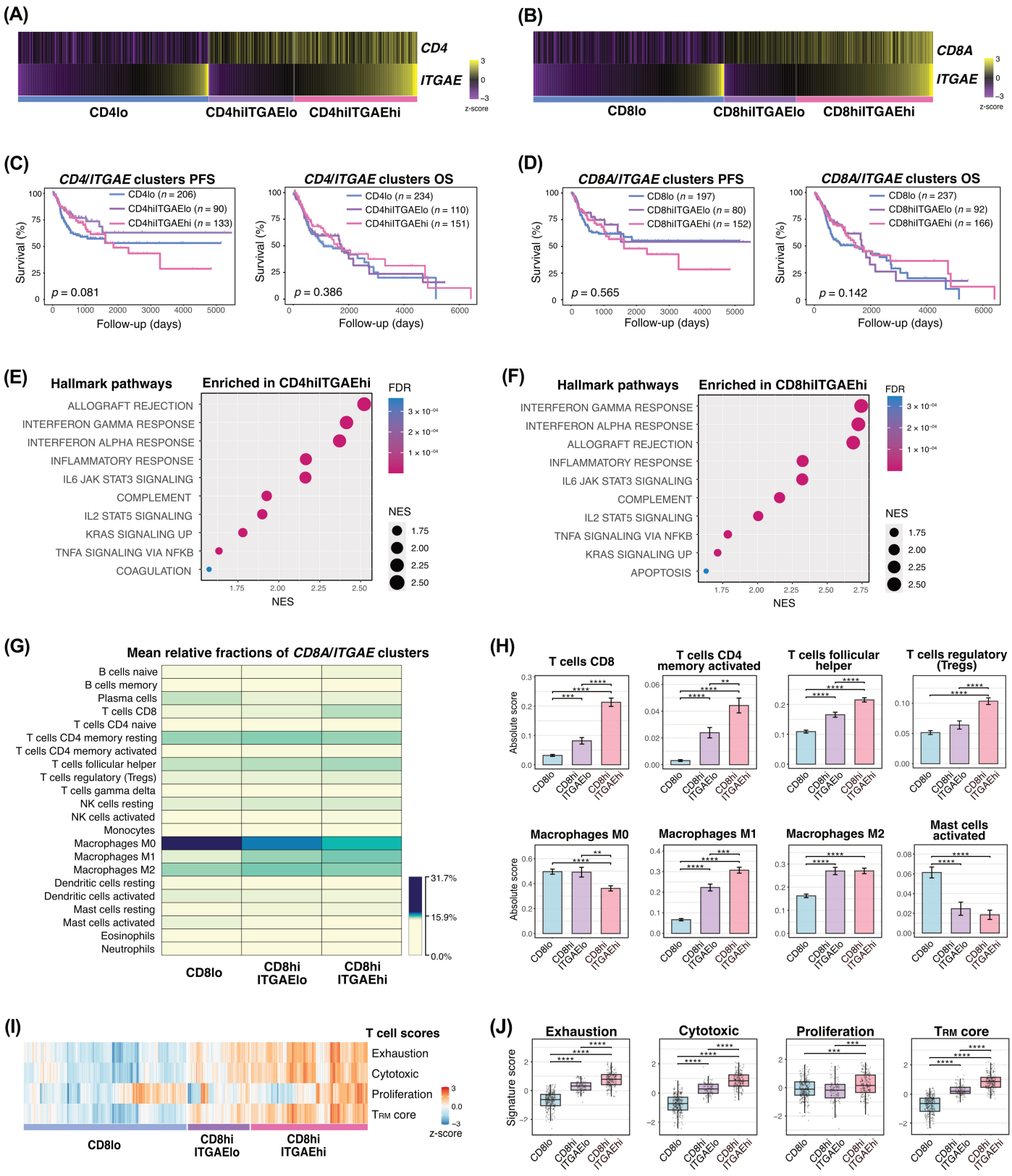

Figure 1. Prognostic and immunological characteristics of *CD4*/*CD8*- and *ITGAE*-defined T-cell states in the TCGA HNSCC cohort. (**A**,**B**) Stratification of patients with HNSCC from the TCGA cohort (n = 520) according to *CD4* (**A**) or *CD8A* (**B**) expression together with *ITGAE* expression. Patients were classified into three groups based on a z-score threshold of 0 for *CD4* or *CD8A* and *ITGAE* expression. (**C**,**D**) Kaplan–Meier analyses of progression-free survival (429 patients, 126 events) and overall survival (495 patients, 190 deaths) according to the *CD4*-based classification (**C**) or the *CD8A*-based classification (**D**). (**E**,**F**) GSEA of Hallmark gene sets comparing the CD4hiITGAEhi with

others (**E**) and CD8hiITGAEhi with others (**F**). The top 10 significantly enriched pathways (FDR < 0.05) are displayed according to NES, with color indicating the FDR. (**G**) Mean relative fractions of the 22 LM22 immune cell types estimated by CIBERSORTx across the *CD8A*-based groups. The color scale shows the group mean for each cell type, expressed as a percentage of the total inferred LM22 immune cell fraction. (**H**) CIBERSORTx absolute scores for eight selected immune cell types across the *CD8A*-based groups. Bars show group means and error bars indicate the standard error of the mean. (**I**) Heatmap showing gene signature scores for exhaustion, cytotoxicity, proliferation, and tissue-resident memory T-cell (TRM) core programs across the *CD8A*-based groups. (**J**) Boxplots of gene signature scores shown in (**I**). HNSCC, head and neck squamous cell carcinoma; TCGA, The Cancer Genome Atlas; GSEA, gene set enrichment analysis; NES, normalized enrichment score; FDR, false discovery rate. **, FDR < 0.01; ***, FDR < 0.001; ****, FDR < 0.0001.

Table 1. Univariate and multivariate survival analyses of PFS in the TCGA cohort.

Variables	Univariate		Multivariate		
	HR (95% CI)	*p*-Value	HR (95% CI)	*p*-Value	FDR
***CD4* model**					
HPV status (ref: negative)					
Positive	0.600 (0.360–1.001)	0.050	0.528 (0.291–0.956)	0.035	
Primary tumor site (ref: oral cavity)					
Larynx	0.757 (0.471–1.217)	0.250	0.570 (0.350–0.926)	0.023	
Hypopharynx	1.886 (0.692–5.139)	0.215	1.673 (0.601–4.658)	0.325	
Oropharynx	0.588 (0.285–1.210)	0.149	0.717 (0.314–1.635)	0.429	
TNM stage (ref: I-II)					
III–IV	1.885 (1.155–3.075)	0.011	2.027 (1.231–3.340)	0.006	
Gene expression					
CD4	0.841 (0.708–0.998)	0.048	0.819 (0.689–0.972)	0.023	0.030
ITGAE	1.139 (0.965–1.345)	0.123	1.292 (1.087–1.536)	0.004	0.007
***CD8A* model**					
HPV status (ref: negative)					
Positive	0.600 (0.360–1.001)	0.050	0.533 (0.292–0.971)	0.040	
Primary tumor site (ref: oral cavity)					
Larynx	0.757 (0.471–1.217)	0.250	0.579 (0.356–0.940)	0.027	
Hypopharynx	1.886 (0.692–5.139)	0.215	1.618 (0.582–4.496)	0.356	
Oropharynx	0.588 (0.285–1.210)	0.149	0.727 (0.317–1.671)	0.453	
TNM stage (ref: I-II)					
III–IV	1.885 (1.155–3.075)	0.011	1.978 (1.198–3.266)	0.008	
Gene expression					
CD8A	0.879 (0.737–1.047)	0.149	0.842 (0.697–1.018)	0.076	0.076
ITGAE	1.139 (0.965–1.345)	0.123	1.318 (1.099–1.582)	0.003	0.007

Abbreviations: TCGA, The Cancer Genome Atlas; PFS, progression-free survival; HPV, human papillomavirus; HR, hazard ratio; CI, confidence interval; ref, reference.

3.2. CD103-Expressing TILs Show Exploratory Survival Associations and Distinct T-Cell Phenotypes

To directly characterize CD103+ T cells within the tumor microenvironment, we performed flow cytometric analysis of TILs from 39 patients with HNSCC. The baseline clinicopathological characteristics and outcome data of the TIL cohort are summarized in Table S5. All 39 patients were HPV-negative, and 35 (89.7%) had hypopharyngeal cancer. All 39 patients in the TIL cohort underwent surgery, either alone (n = 19) or in combination with chemoradiotherapy (*n* = 10), radiotherapy (*n* = 9), or chemotherapy (*n* = 1) (Table S5).

CD103 expression and immune checkpoint molecules were evaluated separately within the CD4⁺ and CD8⁺ T-cell compartments (Figure S2).

We first examined the associations between CD103-expressing TILs and clinical outcomes using Cox proportional hazards regression, treating the proportions of CD103⁺ cells within CD4⁺ and CD8⁺ T-cell populations as continuous variables (Table 2). Among the 39 patients, 17 PFS events and 6 OS events were observed. In the stage-adjusted model, a higher proportion of CD8⁺CD103⁺ TILs showed a nominal association with a lower hazard of progression or death (HR, 0.737; 95% CI, 0.550–0.987; nominal $p = 0.040$), which did not remain statistically significant after BH correction (FDR-adjusted $p = 0.066$). The proportion of CD4⁺CD103⁺ TILs was not significantly associated with PFS in the stage-adjusted model. Neither CD4⁺CD103⁺ nor CD8⁺CD103⁺ TIL proportions showed a statistically significant association with OS in univariate analyses. Stage-adjusted OS estimates were not considered reliable because only six deaths occurred and no deaths were observed among patients with stage II–III disease. The proportional hazards assumption was assessed using Schoenfeld residuals. Global tests showed no statistically significant evidence of violations in the TNM stage-adjusted PFS models for either CD4⁺CD103⁺ ($p = 0.178$) or CD8⁺CD103⁺ T-cell proportions ($p = 0.191$). Given the limited number of events, particularly for OS, these findings should be interpreted as exploratory.

We next examined the relationships between CD103⁺ TIL proportions and clinicopathological characteristics. Neither CD4⁺CD103⁺ nor CD8⁺CD103⁺ TIL proportions were significantly associated with the evaluated clinicopathological characteristics after FDR correction (Table S6).

We further investigated the phenotypic characteristics associated with CD103 expression within tumor-infiltrating T cells. Spearman correlation analysis revealed distinct relationships between the proportions of CD103⁺ cells and other T-cell phenotypes within the CD4⁺ and CD8⁺ compartments (Figure 2). In particular, CD8⁺CD103⁺ TILs showed significant associations with immune checkpoint-related phenotypes, as illustrated by selected correlation plots (Figure 2B). These findings indicate that CD103 expression in intratumoral CD8⁺ T cells is linked to a distinct phenotypic state.

Collectively, these findings suggest that CD103 expression in intratumoral CD8⁺ T cells is associated with distinct immunophenotypic characteristics and may be related to PFS, although the survival findings require validation in larger cohorts.

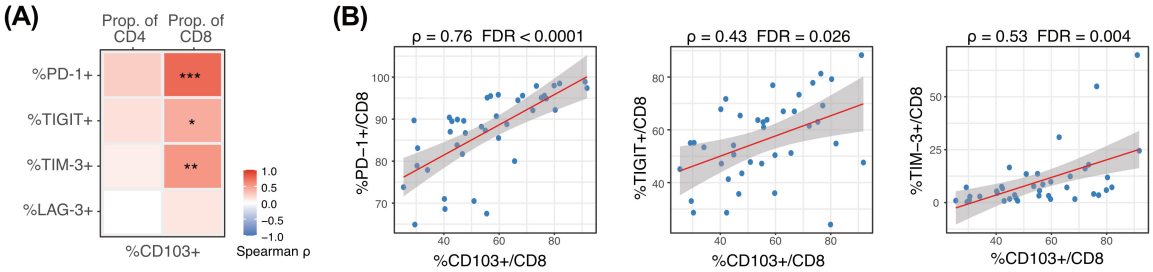

Figure 2. Associations between CD103 expression and immune checkpoint molecule expression in tumor-infiltrating lymphocytes (TILs). (**A**) Heatmap showing Spearman's rank correlation coefficients between the proportions of CD103⁺ cells and other T-cell phenotypes within CD4⁺ TILs or CD8⁺ TILs. (**B**) Scatter plots showing selected correlations shown in (**A**). Each blue dot represents an individual patient sample. Red lines indicate fitted linear regression lines, and gray shaded areas represent 95% confidence intervals. TIL, tumor-infiltrating lymphocyte. *, FDR < 0.05; **, FDR < 0.01; ***, FDR < 0.001.

Table 2. Univariate and multivariate survival analyses of PFS and OS in the TIL cohort.

Variables	Univariate		Multivariate		
	HR (95% CI)	*p*-Value	HR (95% CI)	*p*-Value	FDR
Progression-free survival					
CD4 model					
%CD103⁺ cells/CD4⁺ T cells	0.141 (0.015–1.360)	0.090	0.101 (0.009–1.164)	0.066	0.066
TNM stage IV (ref: II-III)	2.462 (0.562–10.786)	0.232	2.961 (0.665–13.186)	0.154	
CD8 model					
%CD103⁺ cells/CD8⁺ T cells	0.758 (0.564–1.017)	0.065	0.737 (0.550–0.987)	0.040	0.066
TNM stage IV (ref: II-III)	2.462 (0.562–10.786)	0.232	2.956 (0.669–13.066)	0.153	
Overall survival					
CD4 model					
%CD103⁺ cells/CD4⁺ T cells	0.335 (0.008–15.019)	0.574	NE	NE	NE
TNM stage IV (ref: II-III)	NE	NE	NE	NE	
CD8 model					
%CD103⁺ cells/CD8⁺ T cells	0.805 (0.531–1.221)	0.308	NE	NE	NE
TNM stage IV (ref: II-III)	NE	NE	NE	NE	

Stage-adjusted Cox estimates for OS were not reported because no deaths occurred in the stage II–III group, resulting in unstable coefficient estimation. Hazard ratios for CD103⁺ T-cell proportions are expressed per 10-percentage-point increase. Abbreviations: TIL, tumor infiltrating lymphocyte; PFS, progression-free survival; OS, overall survival; HR, hazard ratio; CI, confidence interval; ref, reference; NE, not estimable.

3.3. Circulating CD103⁺ T Cells Show Distinct Clinical and Immunophenotypic Associations in HNSCC

The direct cellular evidence complements the transcriptome-based TCGA findings and supports further investigation of whether CD103⁺ T-cell characteristics are also detectable in the peripheral circulation. We therefore performed flow cytometric analysis of PBMCs from 89 patients with HNSCC. The baseline clinicopathological characteristics and outcome data of the PBMC cohort are summarized in Table S5. Unlike the TIL cohort, the PBMC cohort included both HPV-negative ($n = 51$) and HPV-positive ($n = 38$) patients and a broader distribution of primary tumor sites. The PBMC cohort received heterogeneous treatments, including surgery-based treatment ($n = 52$), concurrent chemoradiotherapy ($n = 17$), and other nonsurgical treatment approaches ($n = 20$) (Table S5). CD103 expression and other T-cell phenotypic markers were evaluated separately within the CD4⁺ and CD8⁺ T-cell compartments (Figure S3A).

We first examined the associations between circulating CD103-expressing T-cell populations and clinical outcomes using Cox proportional hazards regression (Table 3). Among the 89 patients, 41 PFS events and 15 OS events were observed. A higher proportion of CD4⁺CD103⁺ cells among circulating CD4⁺ T cells showed a nominal association with a higher hazard of progression or death in both univariate analysis (HR, 1.295; 95% CI, 1.001–1.676; $p = 0.049$) and the TNM stage-adjusted model (HR, 1.305; 95% CI, 1.007–1.693; nominal $p = 0.044$), which did not remain statistically significant after BH correction (FDR-adjusted $p = 0.089$). In contrast, the proportion of CD8⁺CD103⁺ cells was not significantly associated with PFS in the stage-adjusted model. Neither CD4⁺CD103⁺ nor CD8⁺CD103⁺ T-cell proportions showed statistically significant associations with OS in univariate or stage-adjusted analyses.

We next investigated the relationships between circulating CD103⁺ T-cell proportions and clinicopathological characteristics. CD8⁺CD103⁺ T-cell proportions were significantly associated with HPV status, primary tumor site, T factor, and TNM stage after FDR

correction, whereas CD4⁺CD103⁺ T-cell proportions showed no significant associations with the evaluated clinicopathological characteristics (Table S7).

We further examined the relationships between circulating CD103⁺ T cells and other T-cell phenotypes. Spearman correlation analysis revealed distinct patterns of association within the CD4⁺ and CD8⁺ compartments (Figures 3A,B and S3B). CD103⁺ T-cell proportions were associated with multiple immune checkpoint, activation, proliferation, and differentiation-related phenotypes, indicating that circulating CD103⁺ T cells are linked to broader changes in peripheral T-cell immunophenotypes.

Collectively, these findings suggest that circulating CD103⁺ T cells exhibit clinical and immunophenotypic associations that may differ from those observed in the tumor compartment. The nominal survival associations observed in the TIL and PBMC cohorts warrant further investigation, particularly given their lack of statistical significance after FDR correction and the differences in clinicopathological characteristics between the two cohorts.

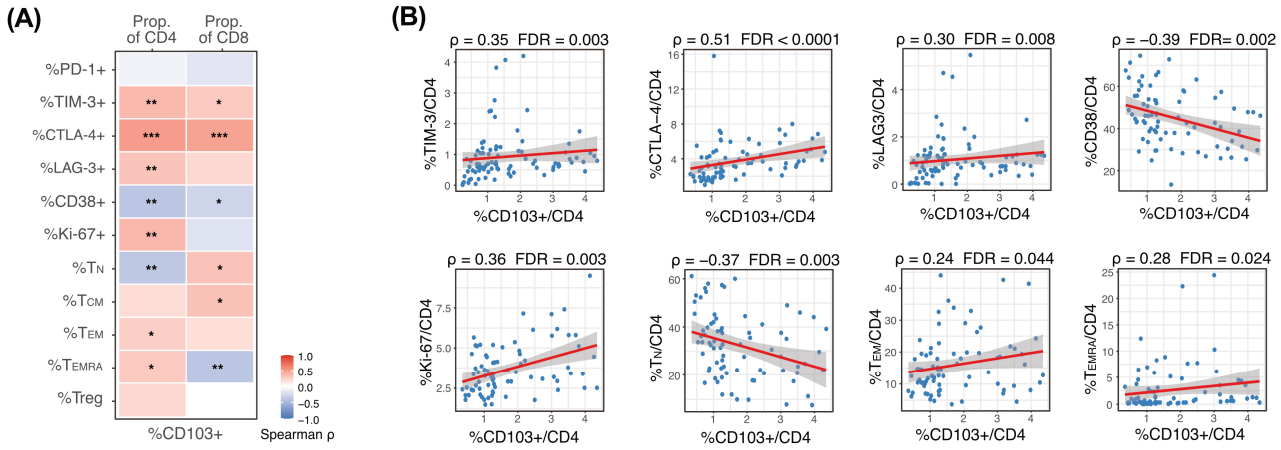

Figure 3. Associations between CD103 expression and immunophenotypic characteristics of peripheral blood T cells. (**A**) Heatmap showing Spearman's rank correlation coefficients between the proportions of CD103⁺ cells and other T-cell phenotypes within CD4⁺ or CD8⁺ T cells. (**B**) Scatter plots showing selected correlations shown in (**A**). Each blue dot represents an individual patient sample. Red lines indicate fitted linear regression lines, and gray shaded areas represent 95% confidence intervals. *, FDR < 0.05; **, FDR < 0.01; ***, FDR < 0.001.

Table 3. Univariate and multivariate survival analyses of PFS and OS in the PBMC cohort.

Variables	Univariate		Multivariate		
	HR (95% CI)	*p*-Value	HR (95% CI)	*p*-Value	FDR
Progression-free survival					
CD4 model					
%CD103⁺ cells/CD4⁺ T cells	1.295 (1.001–1.676)	0.049	1.305 (1.007–1.693)	0.044	0.089
TNM stage III–IV (ref: I-II)	4.909 (2.146–11.234)	0.0002	4.886 (2.146–11.122)	0.0001	
CD8 model					
%CD103⁺ cells/CD8⁺ T cells	0.890 (0.737–1.075)	0.227	0.983 (0.811–1.191)	0.862	0.862
TNM stage III–IV (ref: I-II)	4.909 (2.146–11.234)	0.0002	4.833 (2.074–11.265)	0.0002	
Overall survival					
CD4 model					
%CD103⁺ cells/CD4⁺ T cells	1.313 (0.871–1.979)	0.193	1.323 (0.883–1.982)	0.175	0.351
TNM stage III–IV (ref: I-II)	11.929 (1.565–90.950)	0.017	12.028 (1.579–91.642)	0.016	
CD8 model					
%CD103⁺ cells/CD8⁺ T cells	0.796 (0.558–1.135)	0.207	0.912 (0.639–1.301)	0.610	0.610
TNM stage III–IV (ref: I-II)	11.929 (1.565–90.950)	0.017	10.950 (1.403–85.433)	0.022	

Hazard ratios for CD103⁺ T-cell proportions are expressed per 1-percentage-point increase. Abbreviations: PBMC, peripheral blood mononuclear cell; PFS, progression-free survival; OS, overall survival; HR, hazard ratio; CI, confidence interval; ref, reference.

3.4. CD103⁺ T-Cell Frequencies Differ Between the Peripheral Blood and Tumor Compartments

Given the distinct clinical and immunophenotypic associations of CD103⁺ T cells observed in the tumor and peripheral blood compartments, we directly compared CD103⁺ T-cell frequencies in paired PBMC and TIL samples obtained from 18 patients with HNSCC (Table S5). The proportions of both CD4⁺CD103⁺ and CD8⁺CD103⁺ T cells were significantly higher in TILs than in PBMCs (Figure 4A), demonstrating an increased representation of CD103-expressing T cells within the tumor microenvironment.

We next examined whether the frequencies of circulating CD103⁺ T cells reflected those within the tumor. Among the 18 patients with paired blood and tumor samples, Spearman's ρ for the correlation between circulating and intratumoral CD103⁺ T-cell frequencies was 0.06 (95% CI, −0.35 to 0.48) for CD4⁺ T cells and −0.31 (95% CI, −0.67 to 0.16) for CD8⁺ T cells (Figure 4B). Thus, patients with higher proportions of circulating CD103⁺ T cells did not necessarily have higher proportions of the corresponding CD103⁺ T-cell population within the tumor.

Collectively, these paired analyses demonstrate that CD103⁺ T-cell proportions are higher in the tumor compartment than in peripheral blood, whereas their frequencies in the two compartments were not significantly correlated. These findings suggest that CD103⁺ T-cell populations may exhibit compartment-specific characteristics in HNSCC.

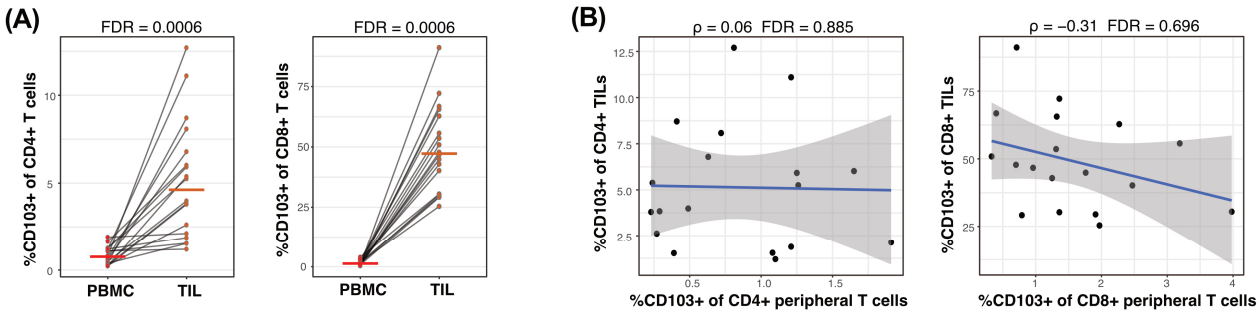

Figure 4. Comparison of CD103⁺ T cells between peripheral blood and TILs. (**A**) Paired comparison of the proportions of CD103⁺ cells among CD4⁺ and CD8⁺ T cells between PBMCs and TILs from the same patients (n = 18). Red and orange horizontal lines indicate the median values for PBMCs and TILs, respectively. Gray lines connect paired samples from the same patients. (**B**) Spearman's rank correlations between the proportions of CD103⁺ cells in peripheral and tumor-infiltrating CD4⁺ or CD8⁺ T cells. Each dot represents an individual patient sample. Blue lines indicate fitted linear regression lines, and gray shaded areas represent 95% confidence intervals.

4. Discussion

In this study, we investigated the clinical and immunological significance of CD103-expressing T cells in HNSCC across transcriptomic, intratumoral, and peripheral blood compartments. In TCGA-HNSCC, higher bulk tumor *ITGAE* expression was associated with a higher hazard of progression or death in models adjusted for *CD4* or *CD8A* expression and clinical covariates. Tumors with high *ITGAE* and high *CD4* or *CD8A* expression also showed enrichment of both effector-associated and immunoregulatory features. Direct analysis of TILs showed a nominal association between a higher proportion of CD8⁺CD103⁺ T cells and a lower hazard of progression or death after adjustment for TNM stage. In contrast, a higher proportion of circulating CD4⁺CD103⁺ T cells showed a nominal association with a higher hazard of progression or death in the stage-adjusted model. The

frequencies of circulating CD103⁺ T cells were not significantly correlated with those in tumors in paired samples. Together, these findings suggest that the clinical and immunological significance of CD103 expression may differ according to T-cell lineage and anatomical compartment.

Our previous study investigated CD69-associated T-cell populations using the same TCGA HNSCC cohort and PBMC samples from 60 patients [15]. In contrast, the present study focused on *ITGAE* (CD103) expression in the TCGA cohort and newly evaluated CD103 expression and its associations with multiple T-cell phenotypic markers in an expanded PBMC cohort of 89 patients, including all 60 patients from the previous study. Furthermore, the present study incorporated analyses of CD103-expressing TILs and paired PBMC–TIL samples, enabling the comparison of CD103-expressing T-cell populations between the tumor and peripheral blood compartments and the evaluation of their distinct clinical associations.

The transcriptomic findings illustrate the complexity of *ITGAE*-associated immune states in HNSCC. Tumor-infiltrating T_{RM}-like cells frequently express inhibitory receptors such as PD-1, TIM-3, TIGIT, and LAG-3 despite retaining features of immune activation and cytotoxicity [17]. Such checkpoint expression does not necessarily indicate complete loss of effector function, but may reflect persistent antigen exposure and the regulatory mechanisms accompanying sustained T-cell activation [17,23]. Indeed, tissue-residency and exhaustion programs can share phenotypic and transcriptional features while representing heterogeneous functional states shaped by the duration and intensity of antigen stimulation [23]. In parallel, the coexistence of effector-associated T-cell populations and regulatory T cells suggests that immune activation and immunoregulatory mechanisms may operate simultaneously within the same tumor microenvironment [24]. Thus, high *ITGAE* expression may be better interpreted as a marker of an immune-engaged tumor microenvironment than as a simple indicator of either effective antitumor immunity or terminal T-cell dysfunction. The TCGA estimate describes the association of bulk *ITGAE* expression with PFS at a given level of *CD4* or *CD8A* expression and the measured clinical covariates. Flow cytometry addressed a different question by measuring the proportion of CD8⁺ TILs expressing CD103 in a separate patient cohort. These differences in measurement and patient populations limit direct comparison of the hazard estimates.

The TIL findings provide direct cellular evidence for the potential clinical relevance of CD103-expressing CD8⁺ T cells within the HNSCC microenvironment. The association between a higher proportion of CD8⁺CD103⁺ TILs and a lower hazard of progression or death in the TNM stage-adjusted model is broadly consistent with previous studies linking CD8⁺ T_{RM}-like cells to improved outcomes in HNSCC and other solid tumors [14–17]. CD103 may be particularly relevant in epithelial malignancies because its interaction with E-cadherin promotes the retention and positioning of T cells within epithelial tissues, facilitating sustained local immune surveillance and tumor-cell interaction [12,13]. CD103-mediated interactions have also been implicated in T-cell migration and cytotoxic activity, providing a potential biological explanation for the association with PFS observed in our cohort [25]. Notably, CD103⁺CD8⁺ TILs can co-express inhibitory receptors while retaining effector potential [17]. Accordingly, the association between CD8⁺CD103⁺ T-cell frequency and immune checkpoint expression in our cohort may reflect persistent tumor engagement and adaptation to the tumor microenvironment rather than terminal dysfunction alone. Whether these cells represent tumor-reactive populations with preserved functional capacity, however, requires direct functional and antigen-specific analyses.

The prognostic significance of CD103 expression was less straightforward within the CD4⁺ T-cell compartment. Although higher proportions of CD4⁺CD103⁺ TILs showed a tendency toward a lower hazard of progression or death, the associations did not reach statistical significance in either univariate or TNM stage-adjusted Cox analyses. This

difference may reflect the greater functional heterogeneity of tissue-resident CD4⁺ T cells. Whereas CD8⁺ TRM cells are commonly associated with local cytotoxic immune surveillance, CD4⁺ tissue-resident populations can encompass conventional helper, cytotoxic, and regulatory phenotypes with different effects on antitumor immunity [18,19,26]. CD103 expression may therefore indicate tissue localization or adaptation without uniquely defining the function of a CD4⁺ T cell. This is particularly relevant in tumors, where CD103 can also be expressed by subsets of regulatory T cells and may contribute to their local retention [18,19]. Thus, the biological consequences of CD103 expression are likely to depend on the lineage and functional program of the cell expressing it, supporting separate evaluation of CD4⁺ and CD8⁺ compartments rather than treating CD103-defined cells as a uniform TRM population.

The peripheral blood findings further extend this context dependency. In the PBMC cohort, a higher proportion of circulating CD4⁺CD103⁺ T cells was associated with a higher hazard of progression or death after adjustment for TNM stage, whereas no statistically significant survival associations were observed for circulating CD8⁺CD103⁺ T-cell proportions. Canonical TRM cells are maintained within tissues by local retention programs and are characterized by limited recirculation; therefore, CD103 expression on circulating T cells cannot be assumed to identify a population functionally equivalent to intratumoral CD103⁺ T cells [20]. Conversely, tissue residency is not necessarily irreversible, and TRM-derived cells can acquire migratory properties [27]. Circulating CD4⁺CD103⁺ T cells may therefore represent heterogeneous populations, potentially including regulatory or chronically activated subsets, which could contribute to their association with unfavorable PFS. The associations between circulating CD8⁺CD103⁺ T-cell proportions and HPV status, primary tumor site, T factor, and TNM stage further suggest that their abundance may be influenced by disease context. Taken together, these findings indicate that circulating CD103⁺ T cells constitute a biologically heterogeneous population whose significance cannot be inferred directly from that of CD103⁺ TILs.

The paired PBMC–TIL analysis further demonstrated differences in the distribution of CD103⁺ T-cell populations between the peripheral blood and tumor compartments. Both CD4⁺CD103⁺ and CD8⁺CD103⁺ T cells were markedly enriched in tumors, consistent with the role of CD103 in tissue retention, whereas no statistically significant correlations were detected between their frequencies in peripheral blood and tumor tissue. Intratumoral TRM populations are shaped by local antigen exposure, tissue-derived signals, and retention cues; for example, transforming growth factor-β can promote CD103 expression and tissue-resident programs, while local antigen recognition can influence TRM differentiation and establishment [20,28]. The intratumoral abundance of CD103⁺ T cells may therefore reflect local recruitment, differentiation, retention, and expansion that are not captured by their frequency in blood. From a biomarker perspective, our paired data did not demonstrate a significant correlation between circulating and intratumoral CD103⁺ T-cell frequencies, suggesting that the utility of circulating CD103⁺ T-cell frequency as a quantitative surrogate for the corresponding intratumoral population requires further investigation. This does not exclude the possibility that other peripheral features, including phenotypic or clonotypic characteristics, may provide information about tumor-associated immune responses. However, these paired observations do not establish compartment-specific differences in prognostic significance, as the survival associations were evaluated in largely distinct TIL and PBMC cohorts.

Several limitations should be acknowledged. First, TCGA analyses relied on bulk transcriptomic data, which cannot establish *CD4*/*CD8A* and *ITGAE* co-expression within individual cells. The z-score threshold of 0 was used for exploratory stratification rather than as a biologically validated cutoff; dichotomization may result in information loss and arbitrary classification of tumors near the threshold. Moreover, expression-based

classifications and CIBERSORTx estimates derived from the same dataset do not provide independent validation. Fewer CD4lo and CD8lo tumors met the CIBERSORTx deconvolution significance threshold than tumors with high expression of both the corresponding T-cell marker and *ITGAE*. This difference may reflect variation in leukocyte abundance or in how well the LM22 reference represents tumor-infiltrating immune-cell states, both of which may affect the comparability of the estimated fractions across groups. Restriction to tumors meeting the threshold preferentially excluded CD4lo and CD8lo tumors and therefore also limits interpretation of the sensitivity analysis. Second, the small TIL cohort, limited paired samples, and few survival events reduced the precision of survival estimates, statistical power, and generalizability. The wide confidence interval for the association between TNM stage and OS in the PBMC cohort further indicates substantial uncertainty. Multivariable analyses adjusted only for TNM stage, leaving potential residual confounding, while differences in HPV status and primary tumor site distributions limit direct cohort comparisons. As $CD103^+$ T-cell proportions were analyzed without outcome-derived cutoff optimization, the survival findings remain exploratory. Although FDR correction was applied to the two lineage-specific survival hypotheses within each cohort and endpoint, the analyses involved multiple cohorts, endpoints, and exploratory comparisons. Therefore, residual multiplicity remains, and the survival findings, particularly those in the smaller TIL and PBMC cohorts, require independent validation. Third, follow-up in the TIL cohort began at surgery, when the specimen was collected, and the findings therefore apply to patients who underwent surgical sampling. In the PBMC cohort, follow-up began at diagnosis. Although all blood samples were collected before treatment, individual collection dates were unavailable. We could therefore neither quantify the interval from diagnosis to sampling nor account for delayed entry. Patients had to survive until blood collection to enter the cohort, and the extent to which this selection and the inclusion of pre-sampling follow-up influenced the PBMC estimates is unknown. Fourth, the absence of healthy PBMC controls precluded assessment of HNSCC specificity. Finally, flow cytometry did not assess tumor-antigen specificity, clonality, or effector function. Because only the TIL panel included a viability dye, residual nonviable cells in the PBMC lymphocyte gate may have influenced the comparison of $CD103^+$ T-cell frequencies between blood and tumor samples. Future studies incorporating single-cell, T-cell receptor, functional, and spatial analyses are warranted.

5. Conclusions

CD103 expression does not define a biologically or clinically uniform T-cell population in HNSCC; rather, its significance depends on both T-cell lineage and anatomical compartment. In the TIL cohort, a higher proportion of $CD8^+CD103^+$ T cells showed a nominal association with a lower hazard of progression or death after adjustment for TNM stage, whereas a higher proportion of circulating $CD4^+CD103^+$ T cells showed a nominal association with a higher hazard in the PBMC cohort. These exploratory findings highlight the importance of cellular and anatomical context when interpreting CD103 expression and warrant validation in larger, independent cohorts.

Supplementary Materials: The following supporting information can be downloaded at: https://www.mdpi.com/article/10.3390/cancers18233817/s1, Figure S1: Immune characteristics of *CD4*-based groups in the TCGA cohort and distributions of *CD4*, *CD8A*, and *ITGAE* expression; Figure S2: Representative flow cytometric gating strategy for tumor-infiltrating lymphocytes (TILs); Figure S3: Representative flow cytometric gating strategy and correlations between CD103 expression and immunophenotypic characteristics of peripheral blood $CD8^+$ T cells; Table S1: Gene sets used for T cell signature scoring [29–34]; Table S2: Antibodies used for flow cytometry; Table S3: Univariate and multivariate survival analyses of OS in the TCGA cohort; Table S4: Association

between *CD4*/*CD8A*- and *ITGAE*-based classifications and clinicopathological features in the TCGA cohort; Table S5: Baseline characteristics of patients in the TIL, PBMC, and paired cohorts; Table S6: Association between the proportion of $CD103^+$ cells and clinicopathological features in the TIL cohort; Table S7. Association between the proportion of $CD103^+$ cells and clinicopathological features in the PBMC cohort.

Author Contributions: Conceptualization, H.T. (Hideyuki Takahashi); data curation, H.T. (Hiroe Tada); formal analysis, H.T. (Hideyuki Takahashi); funding acquisition, H.T. (Hideyuki Takahashi), H.T. (Hiroe Tada) and K.C.; investigation, M.U. and H.H.; methodology, H.T. (Hideyuki Takahashi); project administration, H.T. (Hideyuki Takahashi); resources, K.C.; software, H.T. (Hideyuki Takahashi); supervision, K.C.; validation, H.T. (Hiroe Tada); visualization, H.T. (Hideyuki Takahashi); writing—original draft preparation, H.T. (Hideyuki Takahashi); writing—review and editing, K.C. All authors have read and agreed to the published version of the manuscript.

Funding: This work was supported in part by a Grant-in-Aid for Scientific Research (grant No. 25K02785 (to K.C.), 25K20160 (to Hiroe Tada), and 25K12735 (to Hideyuki Takahashi)) from the Ministry of Education, Culture, Sports, Science, and Technology, Japan.

Institutional Review Board Statement: This study was conducted in accordance with the Declaration of Helsinki, and approved by the Institutional Review Board of Gunma University (No. HS2017-152, approved on 21 June 2016).

Informed Consent Statement: Written informed consent has been obtained from all subjects involved in the study to publish this paper.

Data Availability Statement: The original data presented in this study are openly available on the FireBrowse website, http://firebrowse.org/ (accessed on 6 May 2020). The R scripts, analysis-ready data derived from TCGA-HNSC, and aggregate results from the institutional TIL and PBMC cohorts are publicly available on Zenodo (version 1.1.0, https://doi.org/10.5281/zenodo.24520009). To protect patient confidentiality, individual-level clinical and survival data from the institutional cohorts, patient-level links between TIL and PBMC samples, and raw flow cytometry files are not publicly available.

Conflicts of Interest: The authors declare no conflicts of interest.

Abbreviations

The following abbreviations are used in this manuscript: CI, confidence interval; CTLA-4, cytotoxic T-lymphocyte-associated protein 4; FDR, false discovery rate; GSEA, gene set enrichment analysis; HNSCC, head and neck squamous cell carcinoma; HPV, human papillomavirus; HR, hazard ratio; LAG-3, lymphocyte-activation gene 3; MSigDB, Molecular Signatures Database; NES, normalized enrichment score; OS, overall survival; PBMC, peripheral blood mononuclear cell; PD-1, programmed cell death protein 1; PFS, progression-free survival; ROC, receiver operating characteristic; TIL, tumor-infiltrating lymphocyte; TIM-3, T-cell immunoglobulin and mucin-domain containing-3; TNM, tumor–node–metastasis; T_{RM}, tissue-resident memory T cell.

References

1. Siegel, R.L.; Miller, K.D.; Wagle, N.S.; Jemal, A. Cancer Statistics, 2023. *CA Cancer J. Clin.* **2023**, *73*, 17–48. https://doi.org/10.3322/caac.21763.
2. Nadal, A.; Cardesa, A.; Agaimy, A.; Almangush, A.; Franchi, A.; Hellquist, H.; Leivo, I.; Zidar, N.; Ferlito, A. Massive Parallel Sequencing of Head and Neck Conventional Squamous Cell Carcinomas: A Comprehensive Review. *Virchows Arch.* **2024**, *485*, 965–976. https://doi.org/10.1007/s00428-024-03987-2.
3. Heller, G.; Fuereder, T.; Grandits, A.M.; Wieser, R. New Perspectives on Biology, Disease Progression, and Therapy Response of Head and Neck Cancer Gained from Single Cell RNA Sequencing and Spatial Transcriptomics. *Oncol. Res.* **2023**, *32*, 1–17. https://doi.org/10.32604/or.2023.044774.

4. Chen, Z.; John, J.; Wang, J.H. Why Responses to Immune Checkpoint Inhibitors Are Heterogeneous in Head and Neck Cancers: Contributions from Tumor-Intrinsic and Host-Intrinsic Factors. *Front. Oncol.* **2022**, *12*, 995434. https://doi.org/10.3389/fonc.2022.995434.
5. Borsetto, D.; Tomasoni, M.; Payne, K.; Polesel, J.; Deganello, A.; Bossi, P.; Tysome, J.R.; Masterson, L.; Tirelli, G.; Tofanelli, M.; et al. Prognostic Significance of $CD4^+$ and $CD8^+$ Tumor-Infiltrating Lymphocytes in Head and Neck Squamous Cell Carcinoma: A Meta-Analysis. *Cancers* **2021**, *13*, 781. https://doi.org/10.3390/cancers13040781.
6. Wondergem, N.E.; Nauta, I.H.; Muijlwijk, T.; Leemans, C.R.; van de Ven, R. The Immune Microenvironment in Head and Neck Squamous Cell Carcinoma: On Subsets and Subsites. *Curr. Oncol. Rep.* **2020**, *22*, 81.
7. Kürten, C.H.L.; Kulkarni, A.; Cillo, A.R.; Santos, P.M.; Roble, A.K.; Onkar, S.; Reeder, C.; Lang, S.; Chen, X.; Duvvuri, U.; et al. Investigating Immune and Non-Immune Cell Interactions in Head and Neck Tumors by Single-Cell RNA Sequencing. *Nat. Commun.* **2021**, *12*, 7338. https://doi.org/10.1038/s41467-021-27619-4.
8. Blise, K.E.; Sivagnanam, S.; Banik, G.L.; Coussens, L.M.; Goecks, J. Single-Cell Spatial Architectures Associated with Clinical Outcome in Head and Neck Squamous Cell Carcinoma. *NPJ Precis. Oncol.* **2022**, *6*, 10. https://doi.org/10.1038/s41698-022-00253-z.
9. Wang, D.; Fang, J.; Wen, S.; Li, Q.; Wang, J.; Yang, L.; Dai, W.; Lu, H.; Guo, J.; Shan, Z.; et al. A Comprehensive Profile of $TCF1^+$ Progenitor and TCF1− Terminally Exhausted $PD\text{-}1^+CD8^+$ T Cells in Head and Neck Squamous Cell Carcinoma: Implications for Prognosis and Immunotherapy. *Int. J. Oral. Sci.* **2022**, *14*, 8. https://doi.org/10.1038/s41368-022-00160-w.
10. Schenkel, J.M.; Masopust, D. Tissue-Resident Memory T Cells. *Immunity* **2014**, *41*, 886–897.
11. Gebhardt, T.; Palendira, U.; Tscharke, D.C.; Bedoui, S. Tissue-Resident Memory T Cells in Tissue Homeostasis, Persistent Infection, and Cancer Surveillance. *Immunol. Rev.* **2018**, *283*, 54–76. https://doi.org/10.1111/imr.12650.
12. Topham, D.J.; Reilly, E.C. Tissue-Resident Memory $CD8^+$ T Cells: From Phenotype to Function. *Front. Immunol.* **2018**, *9*, 515. https://doi.org/10.3389/fimmu.2018.00515.
13. Szabo, P.A.; Miron, M.; Farber, D.L. Location, Location, Location: Tissue Resident Memory T Cells in Mice and Humans. *Sci. Immunol.* **2019**, *4*, eaas9673. https://doi.org/10.1126/sciimmunol.aas9673.
14. Hewavisenti, R.; Ferguson, A.; Wang, K.; Jones, D.; Gebhardt, T.; Edwards, J.; Zhang, M.; Britton, W.; Yang, J.; Hong, A.; et al. $CD103^+$ Tumor-Resident $CD8^+$ T Cell Numbers Underlie Improved Patient Survival in Oropharyngeal Squamous Cell Carcinoma. *J. Immunother. Cancer* **2020**, *8*, e000452. https://doi.org/10.1136/jitc-2019-000452.
15. Ida, S.; Takahashi, H.; Kawabata-Iwakawa, R.; Mito, I.; Tada, H.; Chikamatsu, K. Tissue-Resident Memory T Cells Correlate with the Inflammatory Tumor Microenvironment and Improved Prognosis in Head and Neck Squamous Cell Carcinoma. *Oral. Oncol.* **2021**, *122*, 105508. https://doi.org/10.1016/j.oraloncology.2021.105508.
16. Ali, A.; Bari, M.F.; Arshad, S.; Wahid, M.; Safdar, J.; Anwar, K.; Farooqui, W.A. Tissue-Resident Memory T-Cell Expressions and Their Prognostic Role in Head and Neck Squamous Cell Carcinoma: A Systematic Review and Meta-Analysis. *BMC Cancer* **2025**, *25*, 356. https://doi.org/10.1186/s12885-025-13764-2.
17. Corgnac, S.; Boutet, M.; Kfoury, M.; Naltet, C.; Mami-Chouaib, F. The Emerging Role of $CD8^+$ Tissue Resident Memory T (TRM) Cells in Antitumor Immunity: A Unique Functional Contribution of the CD103 Integrin. *Front. Immunol.* **2018**, *9*, 01904. https://doi.org/10.3389/fimmu.2018.01904.
18. Anz, D.; Mueller, W.; Golic, M.; Kunz, W.G.; Rapp, M.; Koelzer, V.H.; Ellermeier, J.; Ellwart, J.W.; Schnurr, M.; Bourquin, C.; et al. CD103 Is a Hallmark of Tumor-Infiltrating Regulatory T Cells. *Int. J. Cancer* **2011**, *129*, 2417–2426. https://doi.org/10.1002/ijc.25902.
19. Hardenberg, J.-H.B.; Braun, A.; Schön, M.P. A Yin and Yang in Epithelial Immunology: The Roles of the αE(CD103)B7 Integrin in T Cells. *J. Investig. Dermatol.* **2018**, *138*, 23–31. https://doi.org/10.1016/j.jid.2017.05.026.
20. Mueller, S.N.; Mackay, L.K. Tissue-Resident Memory T Cells: Local Specialists in Immune Defence. *Nat. Rev. Immunol.* **2016**, *16*, 79–89. https://doi.org/10.1038/nri.2015.3.
21. Mackay, L.K.; Stock, A.T.; Ma, J.Z.; Jones, C.M.; Kent, S.J.; Mueller, S.N.; Heath, W.R.; Carbone, F.R.; Gebhardt, T. Long-Lived Epithelial Immunity by Tissue-Resident Memory T (TRM) Cells in the Absence of Persisting Local Antigen Presentation. *Proc. Natl. Acad. Sci. USA* **2012**, *109*, 7037–7042.
22. Steen, C.B.; Liu, C.L.; Alizadeh, A.A.; Newman, A.M. Profiling Cell Type Abundance and Expression in Bulk Tissues with CIBERSORTx. *Methods Mol. Biol.* **2020**, *2117*, 135–157. https://doi.org/10.1007/978-1-0716-0301-7_7.
23. Gavil, N.V.; Scott, M.C.; Weyu, E.; Smith, O.C.; O'Flanagan, S.D.; Wijeyesinghe, S.; Lotfi-Emran, S.; Shiao, S.L.; Vezys, V.; Masopust, D. Chronic Antigen in Solid Tumors Drives a Distinct Program of T Cell Residence. *Sci. Immunol.* **2023**, *8*, eadd5976. https://doi.org/10.1126/sciimmunol.add5976.

24. Haist, M.; Stege, H.; Grabbe, S.; Bros, M. The Functional Crosstalk between Myeloid-Derived Suppressor Cells and Regulatory T Cells within the Immunosuppressive Tumor Microenvironment. *Cancers* **2021**, *13*, 210. https://doi.org/10.3390/cancers13020210.
25. Le Floc'h, A.; Jalil, A.; Franciszkiewicz, K.; Validire, P.; Vergnon, I.; Mami-Chouaib, F. Minimal Engagement of CD103 on Cytotoxic T Lymphocytes with an E-Cadherin-Fc Molecule Triggers Lytic Granule Polarization via a Phospholipase Cgamma-Dependent Pathway. *Cancer Res.* **2011**, *71*, 328–338. https://doi.org/10.1158/0008-5472.CAN-10-2457.
26. Dong, C.; Lin, L.; Du, J. Characteristics and Sources of Tissue-Resident Memory T Cells in Psoriasis Relapse. *Curr. Res. Immunol.* **2023**, *4*, 100067. https://doi.org/10.1016/j.crimmu.2023.100067.
27. Fonseca, R.; Beura, L.K.; Quarnstrom, C.F.; Ghoneim, H.E.; Fan, Y.; Zebley, C.C.; Scott, M.C.; Fares-Frederickson, N.J.; Wijeyesinghe, S.; Thompson, E.A.; et al. Developmental Plasticity Allows Outside-in Immune Responses by Resident Memory T Cells. *Nat. Immunol.* **2020**, *21*, 412–421. https://doi.org/10.1038/s41590-020-0607-7.
28. Khan, T.N.; Mooster, J.L.; Kilgore, A.M.; Osborn, J.F.; Nolz, J.C. Local Antigen in Nonlymphoid Tissue Promotes Resident Memory $CD8^+$ T Cell Formation during Viral Infection. *J. Exp. Med.* **2016**, *213*, 951–966. https://doi.org/10.1084/jem.20151855.
29. Wherry, E.J.; Kurachi, M. Molecular and Cellular Insights into T Cell Exhaustion. *Nat. Rev. Immunol.* **2015**, *15*, 486–499. https://doi.org/10.1038/nri3862.
30. Scott, A.C.; Dündar, F.; Zumbo, P.; Chandran, S.S.; Klebanoff, C.A.; Shakiba, M.; Trivedi, P.; Menocal, L.; Appleby, H.; Camara, S.; et al. TOX Is a Critical Regulator of Tumour-Specific T Cell Differentiation. *Nature* **2019**, *571*, 270–274. https://doi.org/10.1038/s41586-019-1324-y.
31. Rooney, M.S.; Shukla, S.A.; Wu, C.J.; Getz, G.; Hacohen, N. Molecular and Genetic Properties of Tumors Associated with Local Immune Cytolytic Activity. *Cell* **2015**, *160*, 48–61. https://doi.org/10.1016/j.cell.2014.12.033.
32. Whitfield, M.L.; George, L.K.; Grant, G.D.; Perou, C.M. Common Markers of Proliferation. *Nat. Rev. Cancer* **2006**, *6*, 99–106. https://doi.org/10.1038/nrc1802.
33. Mackay, L.K.; Minnich, M.; Kragten, N.A.; Liao, Y.; Nota, B.; Seillet, C.; Zaid, A.; Man, K.; Preston, S.; Freestone, D.; et al. Hobit and Blimp1 Instruct a Universal Transcriptional Program of Tissue Residency in Lymphocytes. *Science* **2016**, *352*, 459–463.
34. Kumar, B.V.; Ma, W.; Miron, M.; Granot, T.; Guyer, R.S.; Carpenter, D.J.; Senda, T.; Sun, X.; Ho, S.H.; Lerner, H.; et al. Human Tissue-Resident Memory T Cells Are Defined by Core Transcriptional and Functional Signatures in Lymphoid and Mucosal Sites. *Cell Rep.* **2017**, *20*, 2921–2934.

Disclaimer/Publisher's Note: The statements, opinions and data contained in all publications are solely those of the individual author(s) and contributor(s) and not of MDPI and/or the editor(s). MDPI and/or the editor(s) disclaim responsibility for any injury to people or property resulting from any ideas, methods, instructions or products referred to in the content.